Proceedings of ASME Turbo Expo 2023
Turbomachinery Technical Conference and Exposition
GT2023
June 26-30, 2023, Boston, Massachusetts, USA

GT2023-102497

INVESTIGATION ON PROCESS ARCHITECTURES FOR HIGH-TEMPERATURE HEAT PUMPS BASED ON A REVERSED BRAYTON CYCLE

Nancy Kabat
German Aerospace Center
Cottbus, Germany

Enrico Jende
German Aerospace Center
Cottbus, Germany

Eberhard Nicke
German Aerospace Center
Cottbus, Germany

Panagiotis Stathopoulos
German Aerospace Center
Cottbus, Germany

ABSTRACT

Heat pumps are a core technology for the decarbonization of industrial process heat. High-temperature heat pumps (HTHP) typically upgrade waste heat of industrial processes. This way they can simultaneously electrify process heat and reduce the respective primary energy consumption. The utilization of renewable electricity to drive HTHP additionally results in decarbonization of process heat supply. Commercial industrial heat pumps supply process heat at temperatures up to approximately 150°C. However, several studies have shown that process heat can be also supplied with HTHP at temperatures above 150°C. The economic and environmental performance of HTHPs depend strongly on their process architecture and their integration into the industrial process they supply with heat. This paper focuses on the investigation of high-temperature heat pump process architectures based on the reversed Brayton cycle with air as the working medium. The process architecture of the HTHP pilot plant at the Institute of Low-Carbon Industrial Processes of the German Aerospace Center (DLR) is presented and used as a reference. The current work investigates the heat source and heat sink integration in the heat pump cycle architecture and methods to effectively break down the compression and expansion processes to optimize performance for a heat sink temperature of 250°C. To analyze and compare the results, fixed boundary conditions valid for all architectures are made.

Keywords: High-temperature heat pump; Brayton cycle; process architecture; process heat

NOMENCLATURE

COP	Coefficient of performance
C	Compressor
CoBra	DLR pilot plant
DLR	German Aerospace Center
EU	European Union
FED	Final energy demand
GHG	Greenhouse gas
HTHP	High-temperature heat pump
HTHX	High-temperature heat exchanger
HX	Heat exchanger
IHX	Internal heat exchanger
LTHX	Low-temperature heat exchanger
PA	Process architecture
T	Turbine
$\dot{m}$	Mass flow, kg/s
P	Power, kW
p	Pressure, bar
$\dot{Q}$	Heat flow, kW
T	Temperature, K
c_p	Specific heat capacity, kJ/kgK
ε_{HE}	Heat exchanger effectiveness
η_{is}	Isentropic efficiency
ϑ	Temperature, °C
Π	Pressure ratio

1. INTRODUCTION

In order to tackle global warming, the European Union (EU) have committed itself to achieve climate neutrality by 2050 [1]. As an interim target by 2030, greenhouse gas (GHG) emissions are to be at least 55% lower compared to 1990 levels [2]. The industry is the second largest emitting sector with almost 40% of the global final energy consumption. In 2021, fossil fuels still dominate the global final energy consumption whereby about 9,4 Gt of CO_2 was emitted by industry [3]. In order to meet the EU climate targets, a reduction of industrial emissions of more than 7 Gt CO_2 must be achieved by 2030 [3], making the decarbonization of the sector an important step. To assess the heat demand in the industrial sector, several studies have been made. Naegler et al. [4] showed that the total energy demand for process heat in the EU member states in 2012 was 2214 PJ at temperature levels from 100–400°C. Rehfeldt et al. [5] investigated processes in the European industrial sector and found that especially the paper, food and chemical industry have a large demand for process heat in the range of 100°C up to 500°C. Fleiter et al. [6] showed that heating and cooling in the industrial sector represent an important share of the EU final energy demand (FED). The industrial sector accounts of 2390 TWh in 2015, with a process heat account for about 80% FED of heating and cooling. A reduction of the primary energy consumption for industrial process heat can be achieved through the integration of heat pumps driven with renewable energy [7]. Various authors have analyzed the potential of industrial heat pumps for process heat supply. Kosmadakis et al. [8] concluded that industrial heat pumps in the EU industrial sector have a potential of 28,37 TWh/year (102,132 PJ) for waste heat recovery. Wolf et al. [9] analyzed the application of heat pump technology in the EU28 member states industrial sector and found a final energy savings potential of 1,717 PJ, which represents 15% of the industrial final energy consumption. Arpagaus et al. [10] found a technical heat pump potential of about 113 PJ for process heat between 100°C and 150°C in the European market.

The technical feasibility for process heat supply at temperatures of up to 400°C through the use of high-temperature heat pumps (HTHP) was studied by Zühlsdorf et al. [7]. They suggested that the transition to heat pump process heat supply requires further development of the heat pump process and its components' design. Market available heat pumps can supply heat sink temperatures from at least 90°C up to 160°C with COPs between 2,4 and 5,8 and a heating capacity range from about 20 kW to 20 MW [10]. Available heat pump types and technologies have been compared by Wolf et al. [9]. Zühlsdorf et al. [7] showed feasible solutions for process heat supply of up to 280°C. It was suggested a reversed Brayton cycle as a simple construction for applications with large temperature glides. A simultaneous demand for process heating and cooling can be observed in processes such as those found in bakeries [11]. Few studies investigated possible heat pump cycle architectures for process integration. Adamson et al. [12] have presented 49 different high-temperature or trans critical heat pump cycle structures from the literature. Wolf et al. [13] compared several supercritical CO_2 power cycle configurations in terms of thermal efficiency.

Not only the integration of HTHP into an industrial process but also the process architecture itself significantly determines its performance. In the present work, several HTHP process architectures based on the reversed Brayton cycle with air as the working medium are investigated for the first time and compared in terms of their performance for given boundary conditions. A reversed Brayton cycle architecture based on a pilot plant developed at the Institute of Low-Carbon Industrial Processes of the DLR is used as a reference process architecture.

2. HEAT PUMP CYCLE CONFIGURATION

The heat pump process architectures studied are based on the reversed and closed Brayton cycle with air as the working medium.

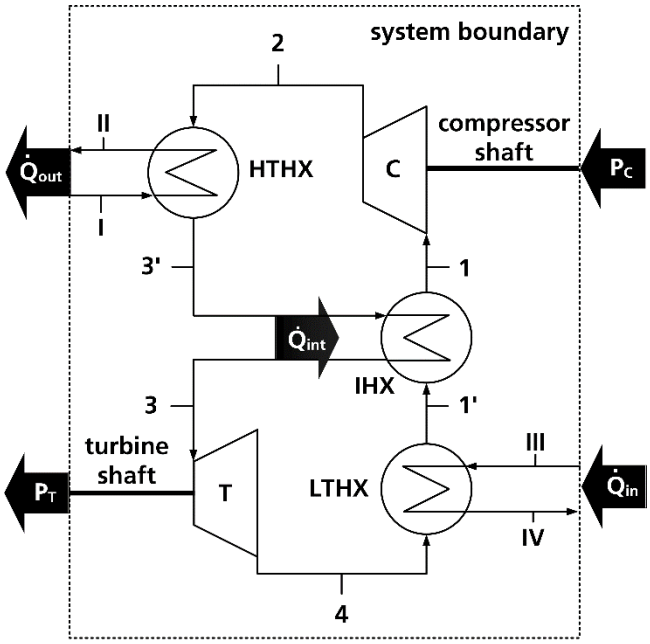

FIGURE 1: SCHEMATIC OF RECUPERATED REVERSED BRAYTON CYCLE BASED ON [14]

For simplicity, in this study the reversed Brayton process is mentioned as the Brayton cycle. In the scheme shown in Fig. 1, arabic numerals represent the parameter measuring points in the Brayton process. The roman numerals represent the parameters for heat source and sink. The Brayton cycle heat pump configuration consists of two heat exchangers (HX), one compressor (C) and one turbine (T). The high-temperature heat exchanger (HTHX) is located at the heat sink while the low-temperature heat exchanger (LTHX) is located at the heat source. The shown cycle configuration was described before by Jende et al. [14] and Schleuss et al. [15]. The working medium is compressed by an electrically driven compressor. Due to the

compression, temperature and pressure of the working medium rise. Sensible heat $\dot{Q}_{out}$ is transferred to the heat sink by the HTHX and the working medium is cooled down. In the present work $\dot{Q}_{out}$ is equated with $\dot{Q}_{sink}$. After the HTHX, the turbine expands the air to temperatures below 0°C and the initial pressure at the compressor inlet. The power generated by the turbine is used to partially drive the compressor. The cycle is closed through the LTHX, whereby the working medium is absorbing the heat from the heat source $\dot{Q}_{in}$. In this work $\dot{Q}_{in}$ corresponds to $\dot{Q}_{source}$. The heat flow transferred can be calculated using the heat flow formula [16] as follows:

$$\dot{Q} = \dot{m} * c_p * \Delta T \quad (1)$$

Due to the high temperatures at the heat sink and the very low temperatures after the turbine, it is possible to provide simultaneous heating and cooling with this heat pump cycle configuration. With an internal heat exchanger (IHX) as an additional component, it is possible to get even lower temperatures after the turbine and higher temperatures before the compressor by internal heat transfer $\dot{Q}_{int}$ [16]. This procedure is further referred to as recuperation. The evaluation of a heat pump system can be made by the efficiency indicator also known as the coefficient of performance (COP) [17]. Arpagaus [17] and Marina et al. [17,18] give a good overview of COP definitions and calculations. The COP indicates the output heating power at heat sink in relation to the applied drive power for the compression. Adapted to the above-described Brayton cycle in Fig. 1 the COP in this study is defined as follows: :

$$COP = \frac{\dot{Q}_{out}}{P} \quad (2)$$

$\dot{Q}_{out}$ indicates the transferred heat flow at the heat sink through the HTHX. The applied drive power for the compression is composed of the difference between the compressor input power P_C and the turbine outlet power P_T. In the current study, simultaneous generation of heating and cooling is assumed, so the total COP is calculated as follows:

$$COP_{total} = \frac{\dot{Q}_{out} + \dot{Q}_{in}}{P_C - P_T} \quad (3)$$

With respect to Eq. 1, the inlet and outlet temperatures ϑ_I and ϑ_{II} at the heat sink are used to calculate the heat flow $\dot{Q}_{out}$. Similarly, the temperatures ϑ_{IV} and ϑ_{III} at the heat source are used to calculate $\dot{Q}_{in}$. The transferred heat flow through the LTHX at the heat source is given by $\dot{Q}_{in}$. Based on the described Brayton cycle, a pilot plant called “CoBra” is developed and build at the DLR Institute of Low-Carbon Industrial Processes. The pilot plant is designed for the working fluids air and argon. Three shell and tube heat exchangers, HTHX, LTHX and IHX, are installed in the system. Furthermore, one axial compressor and one turbine form the turbo component group. The turbomachinery in the DLR pilot plant setup is mechanically decoupled. For more information about the DLR CoBra pilot plant, the reader is referred to the work of Jende et al. [14] and Schleuss et al. [15]. The CoBra pilot plant is used as a reference process architecture in this paper in order to model specific component and boundary conditions. The assumed conditions for the present investigations will be shown in section 3.3.

3. METHODOLOGY

For the present investigations, a matrix of process architectures is created. After that, the system and boundary conditions are set. All investigated process architectures in this study are modeled with the simulation software EBSILON® Professional [19].

3.1 Process architectures

The process architectures studied in this study are all based on the CoBra pilot plant reference architecture without an IHX shown in Fig. 1. For the investigations, the reference architecture is extended by variation of the positioning and the number of turbo machines as well as the heat source and sink integration through heat exchangers. In a first step, the reference architecture without recuperation is extended by the change of position and number of heat exchangers. Thereby only the HTHX and LTHX are adjusted. The number of the heat exchangers is increased from the original two to a total of four. Secondly the number of the heat exchangers remained unchanged at two but the number of turbomachines is varied up to four. Step one and step two are combined so that the number and positioning of both turbomachinery and heat exchangers are changed. In one last step , the integration of an IHX for recuperation is applied to the previous steps. Configurations of two heat exchangers directly in series without separation by turbomachinery or recuperation as well as two turbomachinery directly in series without separation by heat exchangers are not investigated in this work. Process architectures of two single heat exchangers in series are also excluded, since a secondary circuit could provide a higher inlet temperature or one single large heat exchanger could be implemented. Further, a possible high-pressure difference is assumed over a single turbo machine so that no series connection of turbomachinery is needed in this investigation. Both turbomachinery and heat exchanger series implementation are not investigated in this study. Compared to the reference architecture, the following component variations are performed:

- Recuperation (by IHX)
- Intercooled compression (heat sink integration by HTHX)
- Reheated expansion (heat source integration by LTHX)
- Intercooled compression and reheated expansion (by HTHX and LTHX)

The experimental matrix is reduced to finally nine process architectures. The selected and investigated process architectures are presented in the results section.

3.2 Nomenclature of process architectures

To clearly distinguish the various architecture configurations under investigation, a uniform nomenclature is assigned. Each designation starts with the letters PA for process architecture and a number from zero to three. PA0 represents the reference architecture.

After that a combination of the letters C for a compressor and T for a turbine follows and describe the variation of the components in number and arrangement. The order of the letters corresponds to the counterclockwise arrangement of the components in the cycle, starting with the first compressor. Furthermore, this term is combined with the letter R if the architecture is recuperated by an IHX. The more system components are used the longer the expression, e.g., PA3-CCTT-R. Table 1 lists the nomenclature of the investigated process architectures and the combination of components. The number of the integrated HTHX and LTHX can be derived by the number of integrated turbomachinery.

TABLE 1: NOMENCLATURE OF PROCESS ARCHITECTURES

Nomenclature	Number of				
	C	T	HTHX	LTHX	IHX
PA0	1	1	1	1	0
PA0-R	1	1	1	1	1
PA1-R	1	1	1	1	1
PA1-CCT	2	1	2	1	0
PA1-CCT-R	2	1	2	1	1
PA2-CTT	1	2	1	2	0
PA2-CTT-R	1	2	1	2	1
PA3-CCTT	2	2	2	2	0
PA3-CCTT-R	2	2	2	2	1

3.3 Boundary conditions and simulation methodology

Several boundary conditions are applied as given in Table 2 in order to compare all process architectures on equal terms. The study is focused on small HTHP using air as a working fluid and a total thermal output $\dot{Q}_{out}$ between 100 kWth and 200 kWth in order to be able to use component boundary conditions of the DLR pilot plant [14] as a reference point for values of this study. With respect to the pilot plant, a heat sink heat flow of 150 kWth is assumed for the present study. The heat sink and heat source temperatures are assumed based on temperature requirements for bakery processes in the food industry [11]. The bakery process is a good example for the simultaneous demand for process heating and cooling. The temperatures needed in a bakery vary in a range from -30°C to -15°C for deep freezing applications, -5°C for cold storage and +2°C to +7°C for normal cooling [11]. For the baking process, temperatures between 120°C and 280°C

TABLE 2: SYSTEM AND COMPONENT BOUNDARY CONDITIONS

Fixed Parameter	Symbol	Value
Heat sink inlet temperature	ϑ_I	100°C
Heat sink outlet temperature	ϑ_{II}	250°C
Heat sink mass flow	$\dot{m}_{sink}$	0,979 kg/s
Heat sink heat flow	$\dot{Q}_{out}$	150 kW_{th}
Heat source outlet temperature	ϑ_{IV}	-30°C - +5°C
Compressor isentropic efficiency	$\eta_{is,C}$	75%
Turbine isentropic efficiency	$\eta_{is,T}$	85%
Heat exchanger effectiveness	ε_{HE}	90%
Variable Parameter		
Heat source inlet temperature	ϑ_{III}	15°C - 60°C
Heat source mass flow	$\dot{m}_{source}$	max. 2 kg/s
Mass flow Brayton cycle	$\dot{m}_{brayton}$	max. 1 kg/s

are required [11]. Adapted from the bakery requirements, the heat sink outlet temperature ϑ_{II} is set to 250°C and the heat source outlet temperature ϑ_{IV} is varied between -30°C and +5°C in this work. Own assumptions are made for the inlet temperatures of the heat sink and heat source. Assuming that the return flow from an existing furnace process heat can be used to enter the heat sink of the heat pump process, the heat sink inlet temperature ϑ_I is set to 100°C. For the heat source inlet temperature ϑ_{III} variable values between 15°C and 60°C are assumed. These temperatures could be provided by, e.g., waste heat from exhaust gases of the furnace. The integration of the heat pump cycle into the assumed process environment including the temperatures is shown schematically in Fig. 2.

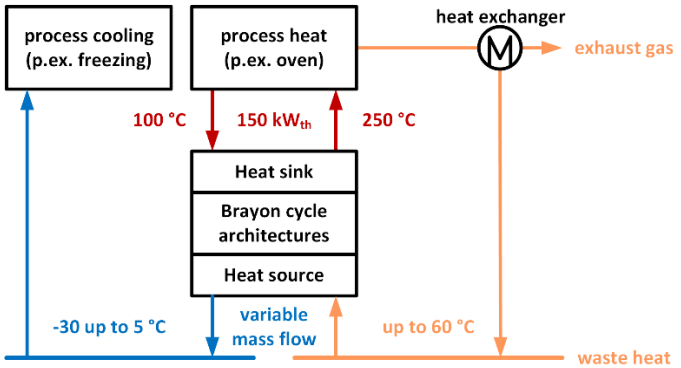

FIGURE 2: PROCESS INTEGRATION FLOW CHART

The heat sink mass flow $\dot{m}_{sink}$ of 0,979 kg/s results from the given heat sink heat flow and the temperatures at the heat sink according to Eq. 1. The effectiveness of all components is assumed constant and have been chosen based on the DLR CoBra pilot plant simulation data. The isentropic efficiencies η_{is} of the turbine and the compressor are assumed to be similar to the efficiencies of the turbomachinery in the operating design of the CoBra pilot plant. In the present work, 75% is assumed for the compressor efficiency and 85% for the turbine efficiency. It

is assumed that the compressor and the turbine are on the same shaft, except for odd numbers of turbo machines. Due to that, the total mechanical power P results from the power balance of each turbo machine.

The heat exchanger effectiveness ε_{HE} is assumed to be 90% also based on the HX effectiveness at the design point of the DLR pilot plant. The mass flow of the heat source $\dot{m}_{source}$ and the Brayton process $\dot{m}_{brayton}$ is assumed to be variable with maximum values for the simulation of the process architectures in this work. A maximum value of 2 kg/s for $\dot{m}_{source}$ and 1kg/s for $\dot{m}_{brayton}$ is set and also based on the operating conditions in the design point of the CoBra pilot plant. In case that the process architecture includes several HX for intercooled compression and reheated expansion, the individual heat flows of $\dot{Q}_{LTHX}$ as well as $\dot{Q}_{HTHX}$ are summed up to ensure only one heat sink and heat source flow per architecture at a time. For process architectures with intercooled compression, the heat sink mass flow is divided into two equal parts before the respective heat exchanger. The split is made in order to avoid too high-pressure ratios between the compressors. The following explains the split in concrete terms. In case of two HTHX in a process architecture, the heat sink mass flow of 0,979 kg/s is divided into two equal mass flows by means of a splitter before the first HTHX. After the split, 0,4895 kg/s flows through HTHX 1 and the other half flows through HTHX 2. Due to the serial arrangement of both HTHX, the heat demand is also halved to 75 kW per HTHX as the mass flow is directly related to the heat flow (Eq.1). Owing to the split heat demand, lower temperatures and thus resulting lower compressors pressure ratios are expected. After HTHX 1 and HTHX 2, the heat sink mass flow is recombined, resulting in a total heat sink heat flow of 150 kW. Further assumptions for the process architecture models are a simplified calculation of turbomachinery without operational maps. The calculation method for heat exchangers is assumed via the effectiveness. No pressure and heat losses in pipelines and components are assumed.

The process architectures with given boundary conditions (Table 2) are simulated with the simulation program EBSILON®. This simulation tool has a very good selection of ready-designed component parts of a heat pump cycle. The simulations are performed to vary ϑ_{IV} in 5°C increments within specified limits between -30°C and 5°C to investigate heat pump efficiencies for all architectures. Fixed simulation parameters are given by the implementation of initial values. Variable simulation parameters are set within predefined limits to target values by means of a controller or an internal optimizer via the actuating variable. The set variable simulation parameters are given in Table 3. COP_{total} is defined as a target function of all simulations and is regulated by using an internal optimizer of the simulation tool. As a target value, the total COP is to be maximized by the use of genetic algorithms with a high number of generations. The number of generations is set to exclude as many random local optima as possible and to find a global optimum. To achieve a fixed temperature of 250°C at the heat sink, the compressor pressure ratios Π_C are regulated between 3 and 25 bar. The temperature at the heat source outlet ϑ_{IV} is regulated by a controller via the parameter $\dot{m}_{source}$ to reach the target temperature. The variation of the temperature between two LTHX is performed by regulating the pressure ratios of the turbines. Since the values for the Brayton mass flow are not known, $\dot{m}_{brayton}$ is always optimized. The control parameter $\dot{m}_{source}$ and the optimization parameter $\dot{m}_{brayton}$ influence each other.

TABLE 3: SIMULATION PARAMETERS

Variable parameter	Controlled parameter (Limits)	Target value
	Regulated by: controller	
ϑ_{II}	Π_C (3 – 25 bar)	250 °C
ϑ_{IV}	$\dot{m}_{source}$ (0,1 – 2 kg/s)	-30°C - +5 °C
ϑ between $LTHX_{1/2}$	p between $turbine_{T1/T2}$ (1 – 25 bar_{abs})	Optimized parameter
	Regulated by: EBSILON® optimizer	
COP_{total}	$\dot{m}_{Brayton}$ (0,3 – 1 kg/s)	Max. COP_{total}
	ϑ_{III} (15 – 60 °C)	
	ϑ between $LTHX_{1/2}$ (15 – 60 °C)	

4. RESULTS AND DISCUSSION

Applying the assumptions explained in chapter 3.1, the experimental matrix is reduced to finally nine process architectures. The nine investigated architectures are shown schematically in Fig. 3. The complexity of the PA increases with the number of components from the reference architecture PA0 up to the most complex PA3-CCTT-R in the present work. A simulation-based parameter study depending on the boundary conditions and simulation method described in chapter 3 is performed. This investigation is carried out to compare the PA with regard to the performance parameter total COP and find an architecture that is more efficient than the reference PA. Due to the large number of PA, an examination of the thermodynamic and economic aspects is not carried out in this work.

As a first result it can be stated that all investigated architectures are able to provide a required heat sink temperature of 250 °C as well as temperatures between -30°C and 5°C at the heat source. All PA are therefore suitable for the simultaneous supply of process heat and cold in the selected boundary condition range.

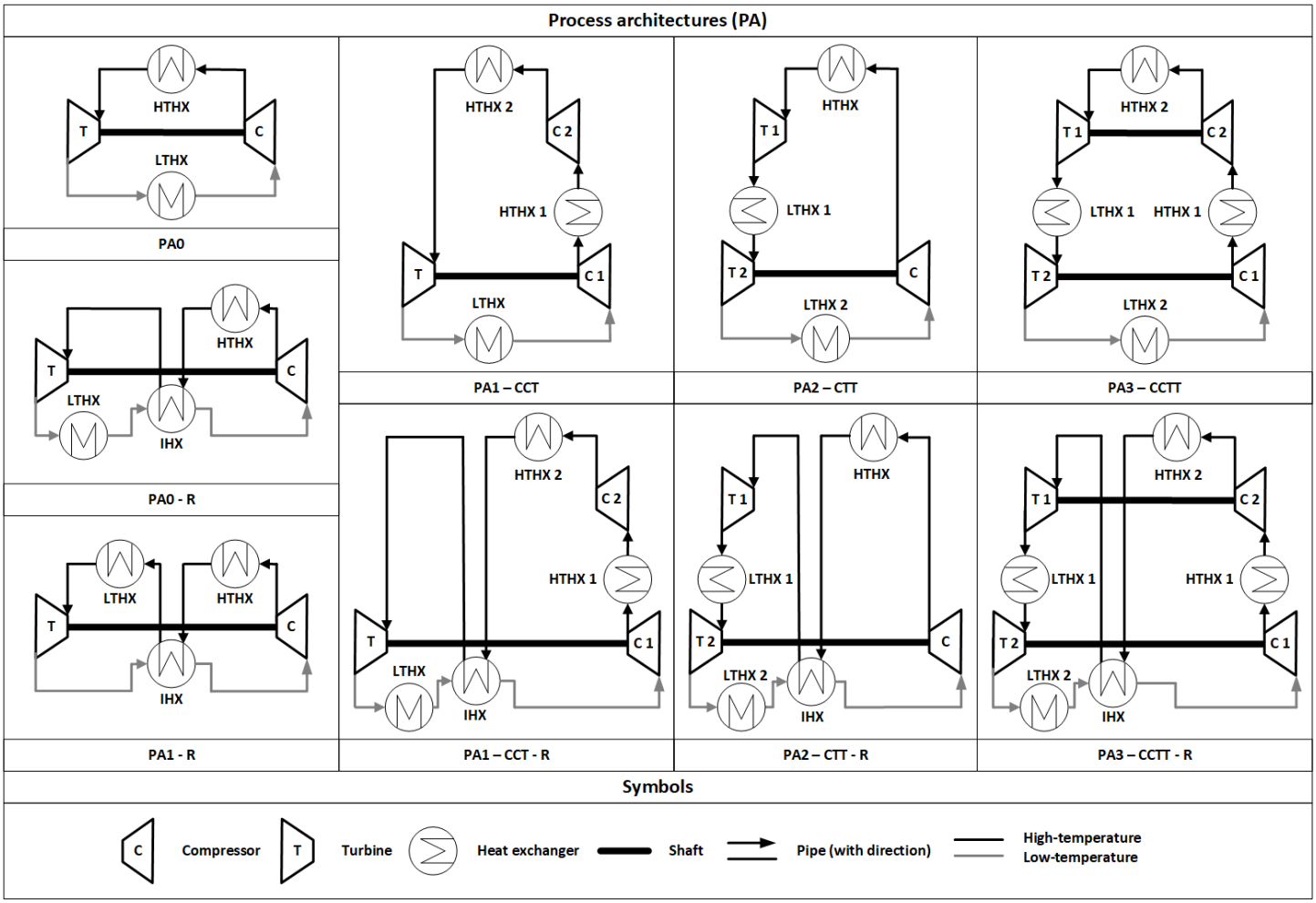

FIGURE 3: SELECTED CYCLE CONFIGURATIONS

Figure 4 presents the total COP for all the nine selected process architectures as a function of the supplied heat.

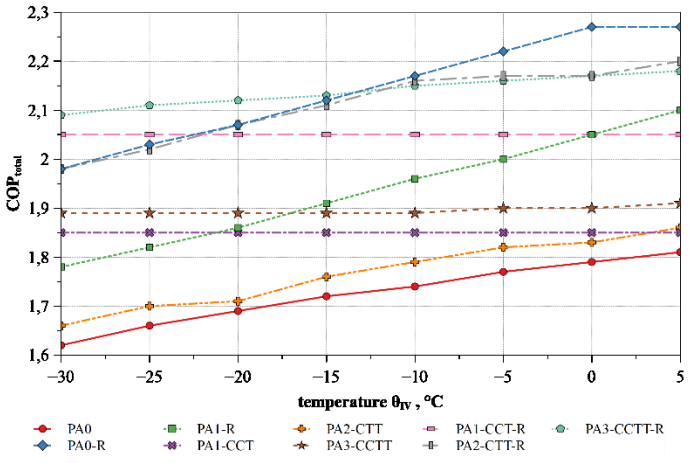

FIGURE 4: TOTAL COP OVER TEMPERATURE

With regard to the total COP, all PA are more efficient than the reference architecture PA0. This result is to be expected, as the integration of an IHX is intended to improve the coefficient of performance. Due to the integration of several turbomachines, the number of HX increase through the use of intercooled compression and reheated expansion. With a higher number of HX, the transferred total heat flow $\dot{Q}$ adds up, which positively influences the total COP according to Eq. 3. With increasing temperature ϑ_{IV}, the total COP increases approximately linearly for all PA except for PA1-CCT, PA1-CCT-R and PA3-CCTT. These three architectures show constant COP_{total} values over the entire temperature range. One factor that all PA with constant COPs have in common is that they have two compressors. As explained in section 3.3, the heat sink mass flow of architectures with more than one compressor is split. Based on the correlations resulting from the temperature change in isentropic changes of state [16] and the heat flow formula (Eq. 1), the lower pressure ratios required at both compressors lead to a lower Brayton mass flow.

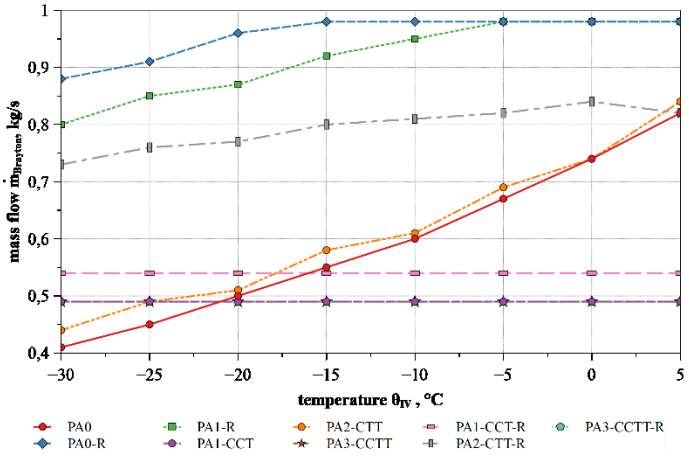

FIGURE 5: BRAYTON MASS FLOW OVER TEMPERATURE

In contrast to other PA, the Brayton mass flow of these three architectures remains constant over the entire temperature range ϑ_{IV}. This can be seen in Fig. 5. The Brayton mass flows of PA1-CCT, PA3-CCTT and PA3-CCTT-R are identical to 0,49 kg/s, therefore the graphs lie on top of each other and are not visible. A constant Brayton mass flow also lead to a constant power requirement of the compressors. The mechanical power P also remains unchanged for all three architectures. In conclusion it can be stated that due to the constant values $\dot{m}_{brayton}$ and P, a constant total COP over the whole temperature range is obtained. In order to establish a detailed comparison, Table 4 lists parameters of four selected PA. Parameters are given for set heat source outlet temperatures at -30°, -15°C, -5°C and 5°C for PA2-CTT, PA1-CCT-R, PA3-CCTT-R and PA0-R. It can be seen that PA1-CCT-R shows approximately constant values except for $\dot{m}_{source}$. The relatively high values from a total COP of 2,05 can be explained by the fact that the heat source heat flow is generally high while P is constantly at 99,241 kW. Under given boundary conditions explained in chapter 3.3, PA1-CCT-R is suitable for use in processes that require a consistently high efficiency over an entire temperature range without fluctuations in the cycle process parameters.

The architecture PA3-CCTT-R also includes two compressors, the COP does not remain constant and shows a slight increase with rising temperature. An explanation could be the additional IHX, which influences the temperature distribution in the system. The pressure ratios Π of the turbomachines are not constant and the total power decreases with increasing ϑ_{IV}. For the examined PA (Fig. 3), COP values between 1,62 and 2,27 can be determined in the given temperature range. For a simultaneous temperature supply of -30°C at the heat source and 250°C at the heat sink the total COP varies between 1,62 for PA0 and 2,09 for PA3-CCTT-R. For a temperature of 5°C total COP values from minimum 1,81 to maximum 2,27 can be found. All architectures with an integrated IHX, except PA1-R in the range of -15°C to -30°C, show higher

TABLE 4: PROCESS PARAMETERS OF SELECTED ARCHITECTURES

	PA2-CTT	PA1-CCT-R	PA3-CCTT-R	PA0-R
		$\vartheta_{IV} = -30$ °C		
$COP(tot)$	1,66	2,05	2,09	1,98
COP	1,32	1,51	1,54	1,48
ϑ_{III}	57,424	60	60	27,279
P	113,89	99,241	97,796	101,312
$\Pi_{C,1}$	12,658	2,376	2,666	2,872
$\Pi_{C,2}$	-	2,242	2,464	-
$\Pi_{T,1}$	2,905	5,327	1,339	2,872
$\Pi_{T,2}$	4,358	-	4,907	-
$\dot{m}_{brayton}$	0,437	0,537	0,49	0,884
$\dot{m}_{source}$	0,422	0,587	0,603	0,884
$\dot{Q}_{LTHX,1}$	4,302	53,101	25,935	50,889
$\dot{Q}_{LTHX,2}$	34,589	-	28,643	-
		$\vartheta_{IV} = -15$ °C		
$COP(tot)$	1,76	2,05	2,13	2,12
COP	1,37	1,51	1,56	1,55
ϑ_{III}	58,055	60	60	41,352
P	109,741	99,241	96,581	96,822
Π_{C1}	7,632	2,374	2,657	2,619
Π_{C2}	-	2,241	2,464	-
Π_{T1}	2,297	5,320	1,563	2,619
Π_{T2}	3,323	-	4,189	-
$\dot{m}_{brayton}$	0,582	0,537	0,49	0,978
$\dot{m}_{source}$	0,587	0,704	0,74	0,978
$\dot{Q}_{LTHX,1}$	0,73	53,101	28,74	55,412
$\dot{Q}_{LTHX,2}$	42,417	-	27,061	-
		$\vartheta_{IV} = -5$ °C		
$COP(tot)$	1,82	2,05	2,16	2,22
COP	1,4	1,51	1,57	1,6
ϑ_{III}	60	60	60	54,419
P	107,449	99,241	95,801	93,844
Π_{C1}	5,947	2,376	2,648	2,596
Π_{C2}	-	2,242	2,464	-
Π_{T1}	2,110	5,327	1,711	2,596
Π_{T2}	2,818	-	3,813	-
$\dot{m}_{brayton}$	0,693	0,537	0,49	0,978
$\dot{m}_{source}$	0,696	0,812	0,866	0,978
$\dot{Q}_{LTHX,1}$	0,361	53,101	29,671	58,395
$\dot{Q}_{LTHX,2}$	45,169	-	26,913	-
		$\vartheta_{IV} = 5$ °C		
$COP(tot)$	1,86	2,05	2,18	2,27
COP	1,41	1,51	1,58	1,62
ϑ_{III}	60	60	60	60
P	106,059	99,241	95,057	92,557
Π_{C1}	4,738	2,375	2,638	2,583
Π_{C2}	-	2,241	2,463	-
Π_{T1}	2,006	5,322	1,853	2,583
Π_{T2}	2,362	-	3,506	-
$\dot{m}_{brayton}$	0,844	0,537	0,49	0,979
$\dot{m}_{source}$	0,851	0,96	1,036	1,079
$\dot{Q}_{LTHX,1}$	0,172	53,101	30,105	59,684
$\dot{Q}_{LTHX,2}$	46,885	-	27,225	-

COP values than the non-recuperated configurations as expected. The positive influence of recuperation for providing very low temperatures is evident (see chapter 2). Due to the internal heat transfer, which results in higher temperatures upstream of the compressor and lower temperatures upstream of the turbine, high compression pressure ratios are not required. The pressure ratios of the individual compressors of PA are illustrated in Fig. 6 and Fig. 7. In accordance with the nomenclature in Fig. 3, the compressor is identified by C1 or C2 after the name of the PA in question. Non-recuperated PA, e.g., PA2-CTT have very high compressor pressure ratios Π_C compared to recuperated PA.

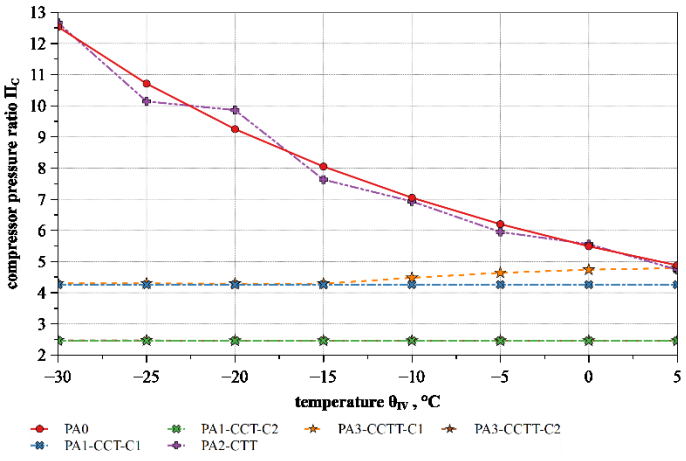

FIGURE 6: COMPRESSOR PRESSURE RATIO FOR NON-RECUPERATED ARCHITECTURES

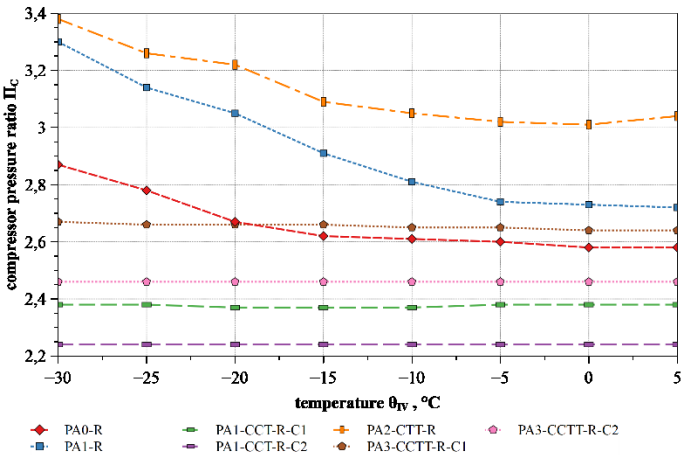

FIGURE 7: COMPRESSOR PRESSURE RATIO FOR RECUPERATED ARCHITECTURES

To provide very low temperatures, non-recuperated process architectures should be avoided and an architecture with an IHX should be preferred. On the basis of the COP results it can be concluded that for low temperatures between -30°C and approximately -15°C the PA3-CCTT-R configuration is best for freeze applications with simultaneous process heat supply of 250°C. The configuration PA0-R seems to be best for temperature supply higher than -15°C, e.g., for use in cold rooms with -5°C or as normal cooling up to 5°C in a bakery.

Architecture PA2-CTT shows the lowest total COP with values between 1,66 and 1,86 compared with the remaining architectures and is the least efficient architecture apart from reference PA0. As a consequence of the reheated expansion, the compressor ratios of this architecture are rather high (Fig. 6). The resulting high overall turbomachinery power, combined with low heat flows at both LTHX, leads to low COP values. In addition, the heat source integration $\dot{Q}_{LTHX,1}$ between both turbines has a very minor influence therefore the additional integration of the LTHX in this architecture is not useful. Considering the PA2-CTT without reheated expansion, the structure would correspond to the structure of the reference architecture PA0, which explains the very similar total COP values of both PA2-CTT and PA0. Due to the lack of recuperation, this architecture is not suitable for the provision of process cooling.

PA3-CCTT-R shows the highest total COP efficiency between -30°C to -15°C with values from 2,09 to 2,18. Due to two compressors, Π_C is constantly low at around 2,5. The graph is approximately constant with a high total COP over the entire temperature range with low values of P and high values of $\dot{Q}_{in}$. The comparison of PA3-CCTT-R with PA0-R shows higher values of COP in the range of -30°C and -15°C and lower COPs in the range of -15°C and 5°C for PA3-CCTT-R. By adding more turbomachinery into the heat pump cycle, the compression and expansion process in the T,S-diagram [16] is shifted closer to isentropic. As this moves the process closer to the ideal cycle, a better COP should result. Due to the lower pressure losses Π, the power output P of PA3-CCTT-R is significantly lower than P of PA0-R in the range of -30°C to -15°C. In this range, the total heat flow at the source is also higher than that of PA0-R. With regard to Eq.3, this leads to higher COP values for PA3-CCTT-R.

At roundabout -12,5°C the graphs for both PA intersect and the COP values of PA0-R are higher than those of PA3-CCTT-R although no additional turbomachines are integrated. One explanation for this occurrence could be the splitting of the heat sink mass flow in PA3-CCTT-R. By splitting the mass flow at the heat sink, a lower heat transfer result. Due to that, the mass flow in the entire system $\dot{m}_{brayton}$ is reduced. This can be seen from the values in Table 4 and the plot of $\dot{m}_{brayton}$ in Fig. 5. PA3-CCTT-R has almost the lowest Brayton mass flow values of all architectures at 0,49 kg/s.

The lower Brayton mass flow leads to a higher temperature at the heat sink, which in turn leads to higher pressure differences resulting in higher values of P. Considering the values in Table 4, it is noticeable that the values of the total power P of PA0-R are always lower than those of PA3-CCTT-R from a temperature of -15°C to +5°C. This corresponds to the fact that higher COP values are achieved with low total outputs and approximately constant heat flows. It seems interesting that a deliberate improvement of the COP due to the integration of several turbomachines and heat exchangers does not seem to be more

promising than a relatively simple PA. A more detailed thermodynamic analysis under variation of the boundary conditions is outside the scope of the investigation carried out here.

The investigation of PA0-R shows, with respect to Table 4, that this is the only architecture that starts with a very low temperature ϑ_{III} of about 27°C to provide cold at -30°C. In the further graph ϑ_{III} increases steadily with a linear rise up to 60°C. Under the given boundary conditions, the optimization of the total COP to provide low heat source temperatures ϑ_{IV} initially results in relatively low heat source inlet temperatures ϑ_{III}. It can be concluded from this that the optimum heat source inlet temperature does not always have to be at 60°C. This also means that the highest possible waste heat temperature ϑ_{III} does not always lead to the highest total COP. This can be explained by the fact that the optimizer aims for low pressure ratios but to generate low temperatures after the turbine, a low heat input in the LTHX and therefore a lower heat source inlet temperature is necessary. With increasing heat source outlet temperatures, this effect is cancelled out, resulting in an increase in P and $\dot{Q}_{in}$. The total COP increases steadily as a result and is highest in the range of approximately -15°C up to 5°C compared to all other architectures.

With respect to the number of components it can be stated that PA0-R with the highest total COP values in the range of -15°C up to 5°C has the lowest number of components compared to the other architectures. The most complex architecture PA3-CCTT-R with the highest number of components, 7 in total, is the most efficient in the very low temperature range from -30°C up to -15°C. For non-recuperated architectures, high pressure ratios are necessary at low required temperatures ϑ_{IV}, therefore it is shown that two compressors lead to a higher efficiency than two turbines, compared for PA1-CCT and PA2-CTT. With the addition of an IHX, this effect is reversed (from -20°C upwards). This effect is not investigated further in this paper.

5. CONCLUSION AND OUTLOOK

An experimental matrix of nine process architectures based on the reversed Brayton cycle was created to investigate the heat source and heat sink integration and methods to effectively break down the compression and expansion processes to optimize performance for simultaneous process heat and cold supply. All results and conclusions apply only to the boundary conditions assumed in this study. This work can serve as a basis for further development of the methodology for analyzing process architectures. The results of this work are limited to the investigation in terms of efficiency due to the large number of architectures.

We found that all investigated architectures are able to provide a heat sink temperature of 250°C as well as temperatures between -30°C and 5°C at the heat source. The results have confirmed that all process architectures studied are more efficient than the reference architecture PA0, which was to be expected due to additional components. The investigations confirm that for the simultaneous provision of process heat and process cooling, architectures with recuperation are to be preferred over non-recuperated. For providing very low temperatures at the heat source, the positive influence of recuperation is evident. The main finding of this study is that in the temperature range between -30°C and -15°C the most efficient process architecture is PA3-CCTT-R with a total COP of throughout about 2,1. In the range of -10°C to 5°C, the most efficient configuration is PA0-R with a total COP of 2,27. The best architecture configuration for freeze applications with simultaneous process heat supply of 250°C is PA3-CCTT-R for low temperatures between -30°C and -15°C. The best configuration for use in cold rooms at -5°C or as normal cooling up to 5°C is PA0-R. In this work, the architecture PA0-R with the lowest number of components has the highest total COP values in the range of -15°C up to 5°C. In contrast, the architecture PA3-CCTT-R with the highest number of components the most efficient in the very low temperature range between -30° and -15°C. A further conclusion from the investigations is that the optimum heat source inlet temperature does not always have to be at 60°C and a high waste heat temperature does not always lead to the highest total COP.

These results can serve as a basis for further investigations. To validate these conclusions listed here, a wider range of boundary conditions should be set up and investigated. Furthermore, a more flexible number of degrees of freedom and variable process parameters up to other requirements regarding the industrial process, e.g., exclusive process heat supply can be investigated. Since an investigation of the thermodynamic and economic aspects is not performed in this work, further investigations could focus on fewer or only one architecture in order to analyze it more specifically.

ACKNOWLEDGEMENTS

The authors thank Jens Gollasch and Robert Hegner.

REFERENCES

[1] Prognos, Öko-Institut, Wuppertal-Institut. “Towards a Climate-Neutral Germany. Executive Summary conducted for Agora Energiewende, Agora Verkehrswende and Stiftung Klimaneutralität.” (10/2020).

[2] Webseite der Bundesregierung | Startseite. “Klimaschutzpaket der EU-Kommission | Bundesregierung.”, 2022. URL https://www.bundesregierung.de/breg-de/themen/europa/fit-for-55-eu-1942402.

[3] IEA. “Industry Materials are the building blocks of society.”, 2022. URL https://www.iea.org/topics/industry.

[4] Naegler, Tobias, Simon, Sonja, Klein, Martin, and Gils, Hans Christian. “Quantification of the European industrial heat demand by branch and temperature level.” *International Journal of Energy Research* Vol. 39 No. 15 (2015): pp. 2019–2030. DOI 10.1002/er.3436.

[5] Rehfeldt, Matthias, Fleiter, Tobias, and Toro, Felipe. “A bottom-up estimation of the heating and cooling demand

in European industry." *Energy Efficiency* Vol. 11 No. 5 (2018): pp. 1057–1082. DOI 10.1007/s12053-017-9571-y.

[6] Tobias Fleiter, Rainer Elsland, Matthias Rehfeldt, Jan Steinbach, Ulrich Reiter, Giacomo Catenazzi, Martin Jakob, Cathelijne Rutten, Robert Harmsen, Florian Dittmann, Philippe Rivière, Pascal Stabat. "Heat Roadmap Europe: EU Profile of heating and cooling demand in 2015." (2017).

[7] Zühlsdorf, B., Bühler, F., Bantle, M., and Elmegaard, B. "Analysis of technologies and potentials for heat pump-based process heat supply above 150 °C." *Energy Conversion and Management: X* Vol. 2 (2019): p. 100011. DOI 10.1016/j.ecmx.2019.100011.

[8] Kosmadakis, George. "Estimating the potential of industrial (high-temperature) heat pumps for exploiting waste heat in EU industries." *Applied Thermal Engineering* Vol. 156 (2019): pp. 287–298. DOI 10.1016/j.applthermaleng.2019.04.082.

[9] Wolf, S. and Blesl, M. "Model-based quantification of the contribution of industrial heat pumps to the European climate change mitigation strategy." *ECEEE Ind Summer Study Proc* (2016): 477-87.

[10] Arpagaus, Cordin, Bless, Frédéric, Uhlmann, Michael, Schiffmann, Jürg, and Bertsch, Stefan S. "High temperature heat pumps: Market overview, state of the art, research status, refrigerants, and application potentials." *Energy* Vol. 152 (2018): pp. 985–1010. DOI 10.1016/j.energy.2018.03.166.

[11] Dipl.-Ing.Jörg Schulz. "Leitfaden"Energieeffizienz in Bäckereien - Energieeinsparungen in Backstube und Filialen".", 2014. URL https://www.selbstaendig-im-handwerk.de/downloads/News/EnEffBaeckerei-Leitfaden-Juli2014.pdf.

[12] Adamson, Keri-Marie, Walmsley, Timothy Gordon, Carson, James K., Chen, Qun, Schlosser, Florian, Kong, Lana, and Cleland, Donald John. "High-temperature and transcritical heat pump cycles and advancements: A review." *Renewable and Sustainable Energy Reviews* Vol. 167 (2022): p. 112798. DOI 10.1016/j.rser.2022.112798.

[13] Veronika Wolf. "Investigation of sCO2 Cycle Layouts for the Recovery of Low Temperature Heat Sources." Paper #42, San Antonio, Texas (2022). URL https://sco2symposium.com/proceedings2022/042-paper.pdf.

[14] Jende, Enrico, Schleuss, Leander, Oehler, Johannes, and Nicke, Eberhard. "Entwicklung und Aufbau von Hochtemperatur-Wärmepumpen zur Integration regenerativer Energieträger in industrielle Prozesse und thermische Speicherkraftwerke.": pp. 225–236. Dresden, Deutschland, 18.-19. Okt. 2022.

[15] L. Schleuss, T. Lorenz, D. Wenzke, C. Hensel, S. Panagiotis, E. Nicke, and U. Riedel. "Decarbonisation of industrial processes - new dlr institute in cottbus and zittau.", Conference proceedings of the 4th international conference on energy supply and energy efficiency and "5 years NESEFF" (2020).

[16] Böckh, Peter von and Stripf, Matthias. *Technische Thermodynamik: Ein beispielorientiertes Einführungsbuch*. Springer Berlin Heidelberg, Berlin, Heidelberg (2016).

[17] Arpagaus, Cordin. *Hochtemperatur-Wärmepumpen: Marktübersicht, Stand der Technik und Anwendungspotenziale*. VDE Verlag GmbH, Berlin, Offenbach (2019).

[18] Marina, A., Spoelstra, S., Zondag, H. A., and Wemmers, A. K. "An estimation of the European industrial heat pump market potential." *Renewable and Sustainable Energy Reviews* Vol. 139 (2021): p. 110545. DOI 10.1016/j.rser.2020.110545.

[19] STEAG Ebsilon. "STEAG EBSILON.", 2022. URL https://www.ebsilon.com/de/.